Chemical Engineering Research and Design 130 (2018) 199–207

Contents lists available at ScienceDirect

Chemical Engineering Research and Design

journal homepage: www.elsevier.com/locate/cherd

Improving oxygen transfer efficiency by developing a novel energy-saving impeller

Zhiyong Zheng[a,*], Dongdong Sun[a], Jing Li[b], Xiaobei Zhan[a], Minjie Gao[a]

[a] Key Laboratory of Industrial Biotechnology, Ministry of Education, School of Biotechnology, Jiangnan University, Wuxi 214122, Jiangsu Province, China
[b] School of Environmental and Biological Engineering, Nanjing University of Science and Technology, Nanjing 210094, Jiangsu Province, China

ARTICLE INFO

Article history:
Received 12 July 2017
Received in revised form 7 December 2017
Accepted 11 December 2017
Available online 21 December 2017

Keywords:
Gas dispersion
Impeller
Energy saving
Efficient oxygen transfer

ABSTRACT

Radial flow impeller is the energy-intensive and fundamental component in reactors for the gas–liquid transfer process. A newly designed fan-shaped turbine (FT) assembly with annular-sector-shaped concave blades was characterized and compared with the Rushton turbine (RT) and Bakker turbine (BT). A new surface equation was established to design the blade of the FT impeller. Under turbulence conditions, the FT impeller showed a lower power number and higher relative power demand (RPD) compared with RT and BT impellers. The power number of the FT impeller was 1.7, lower by 26% than that of BT impeller. The RPD of the FT impeller was nearly 0.95 at a high impeller speed. The critical dispersion speed, gas holdup, and volumetric oxygen transfer coefficient of the FT impeller were close to those of BT impeller. Moreover, the oxygen transfer efficiency of the FT impeller was remarkably higher by 35%–66% and 23%–34% than that of RT and BT impellers, respectively. The FT impeller showed competence in a broad operation range, strong robustness, energy-saving feature, and efficient mass transfer characteristics.

1. Introduction

Gas dispersion is widely used in aeration, oxidation, chlorination, and hydrogenation processes in industrial applications of aerobic fermentation, environmental engineering, and chemical engineering. Gas dispersion is mostly achieved through agitation, which breaks large bubbles into small bubbles in fluids, thereby promoting gas-to-liquid mass transfer (Bakker et al., 1994). Radial flow impellers are the most commonly used type of impeller, and they are the main energy-consuming component of a gas dispersion unit. To reduce energy consumption during aeration and agitation, engineers often combine gas–liquid dispersion (employed in radial flow impellers) with mixing (employed in axial flow impellers) to construct an efficient gas–liquid reaction system (Gogate et al., 2000). The power input required for a gas dispersion impeller commonly accounts for 40%–70% of the power input of an entire agitation system. Therefore, developing efficient and energy-saving impellers is urgently needed to improve gas dispersion process.

Rushton et al. (1950) designed the first flat-blade impeller (Rushton turbine, RT) in the 1950s. RT became the standard impeller used in gas–liquid dispersion processes for a long time. The impeller is usually assembled with six blades on a disc and thus called RT-6. Although the RT impeller displays a simple structure and good gas dispersion, it requires high power input and brings strong shear force. In the 1970s, Van't Riet and Smith (1975) found that trailing vortexes produced behind the RT-6 impeller blades is the main cause of energy wastage. Cavities are formed when the trailing vortex is filled with gas under gassed condition. The presence of cavities results in unstable power consumption and reduced mass transfer efficiency during gassed agitation. Van't Riet et al. (1976) subsequently developed an impeller assembly consisting of semi-circular tube blades (concave disc turbine, CD), which greatly reduced cavitation and improved the efficiency of gas–liquid mass transfer. Analysis has shown that the formation of flow patterns varies between RT impeller and CD-6 impeller (Devi and Kumar, 2013). Since then, researchers have developed a series

* *Corresponding author.*
E-mail addresses: zhiyong@jiangnan.edu.cn (Z. Zheng), 1115014295@qq.com (D. Sun), lijing2031447@163.com (J. Li), xbzhan@jiangnan.edu.cn (X. Zhan), gaominjie@msn.com (M. Gao).
https://doi.org/10.1016/j.cherd.2017.12.021
0263-8762/

Nomenclature

C_L	Dissolved oxygen concentration (g/L)
C_L*	Saturated dissolved oxygen concentration (g/L)
D	Impeller diameter (m)
d	Disc diameter (m)
E	Oxygen transfer efficiency (m^3/J)
H	Liquid loading height (m)
H_g	Liquid height under gassed condition (m)
h	Upper or lower blade height (m)
h_1	Upper blade height (m)
h_2	Lower blade height (m)
k_{1-6}	Constant
k_La	Mass transfer coefficient (1/s)
L	Blade radial length (m)
m	Torque (N·m)
N	Impeller speed (r/s)
N_L	Critical dispersed speed (r/s)
N_p	Power number
n	Blade number
P_A	Power of aeration (W)
P_g	Power under gassed condition (W)
P_u	Power under ungassed condition (W)
Q_g	Gas flow rate (L/min)
Re	Reynolds number
r	Impeller radius (m)
T	Tank inner diameter (m)
t	Measurement time (s)
V_L	Liquid volume in the tank (m^3)
v_s	Superficial gas velocity (m/s)
W_1	Upper blade width (m)
W_2	Lower blade width (m)

Greek symbols

δ	Blade thickness (m)
ε	Gas holdup (%)
ρ	Liquid density (kg/m^3)
Ψ	Tangential radian of FT blade (rad)

Abbreviations

BT	Bakker turbine
DO	Dissolved oxygen
FT	Fan-shaped turbine
RPD	Relative power demand
RT	Rushton turbine

of impeller assemblies with deeper concaved blades, such as Gasfoil (Hjort and Skanberg, 1988) and Scaba 6SRGT (Galindo and Nienow, 1993; Middleton and Ramshaw, 1993) impellers in the 1980s and 1990s, respectively. Bakker (1998) invented an impeller assembly with asymmetric concave blades (Bakker turbine, BT). The BT impeller presents two advantages: (1) the parabolic-shaped blade has a more curved vertex than the other impeller blades, resulting in weaker cavitation effect; and (2) the upper portion of the blade above the disc hangs over the lower portion to facilitate the capture and dispersion of gas. RT, CD, and BT impellers are widely used in industrial processes, and BT impeller is currently the most efficient radial flow impeller.

We recently designed a new radial flow impeller (Zheng et al., 2017), in which the blade surface employs a new equation (Eq. (1)). The generatrix of the blade in the peripheral direction could be seen as spatial curves of parabola that fit the cylindrical surface. The surface extends the tangential width of the blade without changing the diameter of the impeller. Furthermore, the blade is fan-shaped (annular sector) as projected on the horizontal plane, hence the name fan-shaped turbine (FT). The torque in the outer edge of the blade is high, so the outer side of the blade was designed to have a deeper concave shape, which can possibly reduce power consumption. The extended tangential width and the increased blade area ensure good performance for gas capture and gas dispersion. In the present work, our main purpose is to characterize the agitation and gas dispersion performance of the FT impeller. We carried out an experimental investigation and compared this impeller with the traditional RT and BT impellers.

2. Materials and methods

2.1. Impellers

Three impellers with the same diameter, i.e. BT, RT, and the newly designed FT, were investigated in this work. The surface equation of the FT blade is

$$z = \frac{h}{\Psi^2}\left(\arctan\frac{y}{x}\right)^2$$
$$x \in [r-L, r], \quad y \in [(r-L)\cdot\sin\Psi, r\cdot\sin\Psi] \tag{1}$$

where h is the upper or lower blade height, Ψ is the tangential radian of the annular sector (the blade projection on the horizontal plane), r is the radius of the impeller, and L is the length of the blade. x, y, and z refer to the three-dimensional coordinates.

The schematic diagram top-view of the three impeller blades in one disc is shown in Fig. 1. The three impellers were plotted using SolidWorks software and printed by a 3D printer (US Stratasys Fortus 250mc) using ABS Plus plastics. The blade was 3 mm thick. The mechanical strength of the blade met the test requirements as revealed in the pre-experiments. Fig. 2 shows the photographs of the three impellers used in the experiments.

Except for the shape of the blades, the impeller diameter, disc diameter, blade length, and blade height of the three impellers were similar. The dimensions of the impellers are presented in Table 1.

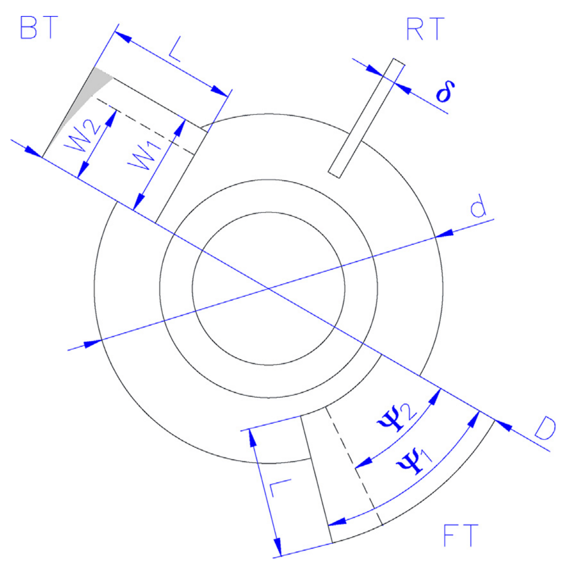

Fig. 1 – Schematic diagram top-view of the three impeller blades in one disc. Gray area in BT blade was speculated to be a low efficiency region for gas dispersion.

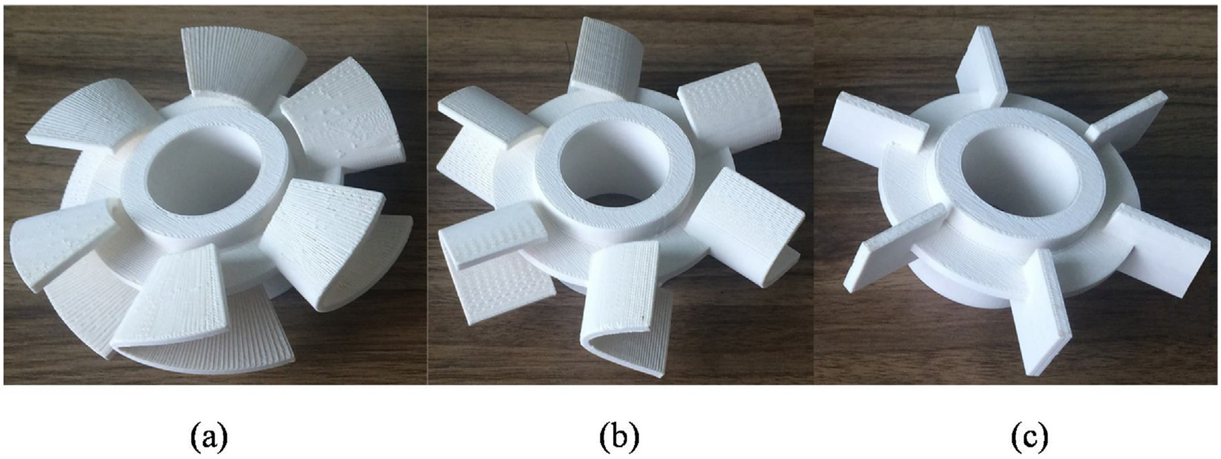

Fig. 2 – Photographs of the three 3D printed impellers (bottom view). (a) FT impeller; (b) BT impeller; (c) RT impeller.

Table 1 – Dimensions of the three impellers.

Dimension	Value
Impeller diameter, D	0.12 m
Disc diameter, d	0.08 m
Blade number, n	6
Blade radial length, L	0.03 m
Blade height, $h_1 + h_2$	0.024 m
Blade thickness, δ	0.003 m
Blade width (BT only), W_1, W_2	0.024 m (upper), 0.018 m (lower)
Blade tangential radian (FT only), Ψ_1, Ψ_2	0.8 rad (upper), 0.6 rad (lower)

Note: The dimensions correspond to the parameters in Fig. 1.

2.2. *Stirred tank reactor*

As shown in Fig. 3, a transparent stirring tank was used to characterize the performance of the impellers. A motor and a reducer rendered the rotational speed stable and adjustable. Compressed air was blown out from the orifices found on the gas sparger, and the gas flow rate was measured and adjusted by a rotameter. A torque meter (GB-DTS, Beijing Landmark Sensor Technology Co., Ltd., China) and a dissolved oxygen (DO) electrode (InPro 6860i, Mettler Toledo, Switzerland) were used to measure the torque during agitation and the DO concentration in the water. The tank comprises a standard elliptical head at the bottom and four evenly distributed baffles. Fig. 3b and c shows the positions of the baffle and the DO electrode. The part of the setup found below the liquid level is shown in Fig. 3c, and their sizes are indicated in Table 2.

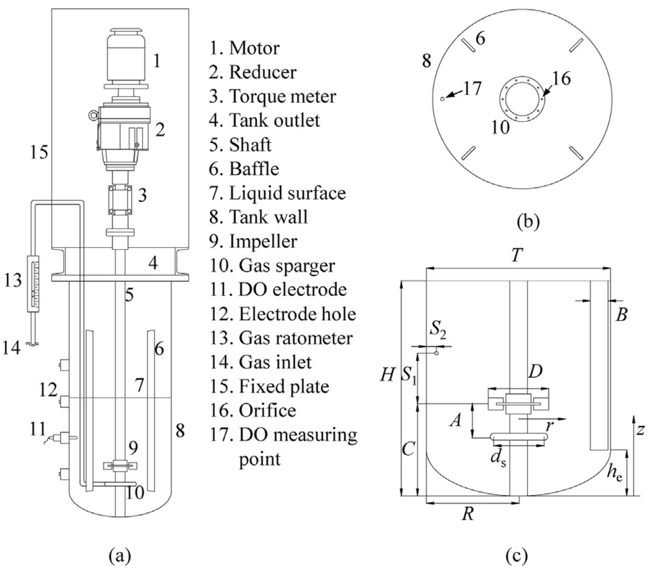

Fig. 3 – Schematic of the experimental setup. (a) Components of the set; (b) Top view; (c) Size of the stirred tank reactor set up.

2.3. *Operating conditions*

The experiment was performed in an air–water system as described in the text. Air was supplied by an air compressor, and the gas flow rate (Q_g) was 0–120 L/min. The impeller speed (N) was set at 3–8 r/s. The liquid bulk temperature was 20 °C.

2.4. *Methods*

Power P during agitation is calculated by the following equation (Nienow, 1990):

$$P = 2\pi N m \tag{2}$$

where P is the power, N is the impeller speed, and m is the torque.

Relative power demand (RPD) is the ratio of the power draw of the impeller under gassed condition (P_g) to the ungassed power draw (P_u) (Smith and Gao, 2001). For the determina-

Table 2 – Dimensions of the stirred tank reactor setup.

Dimension	Value (m)
Tank inner diameter, T	0.366
Liquid loading height, H	0.427
Gas sparger diameter, d_s	0.080
Orifice diameter, d_h	0.003
Baffle width, B	0.035
Distance between the impeller and the bottom of the tank, C	0.183
Distance between the impeller and the sparger, A	0.060
Vertical distance between the DO measuring point and the impeller, S_1	0.100
Horizontal distance between the DO measuring point and the impeller, S_2	0.020
Elliptical head height, h_e	0.092

Note: The dimensions correspond to the parameters in Fig. 3.

tion of RPD (= P_g/P_u), impeller rotation was started prior to gas entry, with the gas flow being progressively increased from zero to the maximum flow rate.

The critical dispersion speed was determined through visual inspection (Fasano et al., 2011). The gas flow was first maintained at a certain rate. Second, the impeller speed was progressively increased from zero to a certain speed, at which gas bubbles started to reach the tank wall corresponding to the horizontal level of the impeller disc. This minimum speed was recorded and considered as the critical dispersion speed.

Gas holdup ε was calculated based on the changes in liquid level under ungassed and gassed conditions. The equation is as follows:

$$\varepsilon = \frac{\pi T^2 \left(H_g - H\right)/4}{\pi T^2 \left(H_g - H\right)/4 + V_L} \tag{3}$$

where T is the inner diameter of the tank, and H_g is the liquid height under gassed condition. H is the liquid loading height under ungassed condition. V_L is the liquid volume in the tank.

H_g was difficult to read accurately when the fluid was gassed and agitated. High-speed camera was used to instantaneously record the liquid level after the flow field stabilized. More than 50 photos were obtained to determine the liquid level, and the average reading was calculated.

Volumetric oxygen transfer coefficient (k_La) was measured using a classic dynamic method. In this case, the conventional procedure was implemented in the experimental analysis: first, the dissolved oxygen was removed through nitrogen sparging. Subsequently, a step change in air flow was introduced by sharply increasing the oxygen flow rate using a pair of alternating magnetic valves. Basically, k_La is the slope of a semi-logarithmic plot $\ln(C_L^* - C_L)$ versus time t (Garcia-Ochoa and Gomez, 2009) as follows:

$$k_La = -\frac{\ln\left(C_L^* - C_L\right)}{t} \tag{4}$$

where k_La is the volumetric oxygen transfer coefficient, C_L^* is the saturated dissolved oxygen concentration, C_L is the dissolved oxygen concentration at real time, and t is the measurement time. The measurement was repeated three times. We also employed the probe response time correction model proposed by Garcia-Ochoa and Gomez (2009) to correct k_La value.

Oxygen transfer efficiency E is expressed as the volumetric oxygen transfer coefficient per unit volume of power consumption under aeration conditions, as follows:

$$E = \frac{k_La}{P_g/V_L} \tag{5}$$

where E is the oxygen transfer efficiency, P_g is the gassed power, and V_L is the liquid volume.

3. Results and discussion

3.1. *Power number*

Power is an important parameter in industrial processes, and it affects equipment investment and operating costs. In designing fermenters and other agitated reactors, power is the key process parameter that must be determined in advance (Tervasmäki et al., 2016). Power is not only related to impeller type and size but also to factors such as reactor scale, liquid viscosity, density, solid content, and gas holdup. Power number (N_P) represents the power characteristics of an impeller based on angular momentum balance. Moreover, power number is one of the most widely used design parameters in mixing operation. Power number is a function of the Reynolds number for an impeller. When Reynolds number in a flow field is greater than 10,000, i.e., full turbulence state has been reached, the power number tends to be a constant (Bakker et al., 1994). N_P is calculated by

$$N_P = \frac{P_u}{\rho N^3 D^5} \tag{6}$$

where P_u is the ungassed power, ρ is the liquid density, N is the impeller speed, and D is the diameter of the impeller.

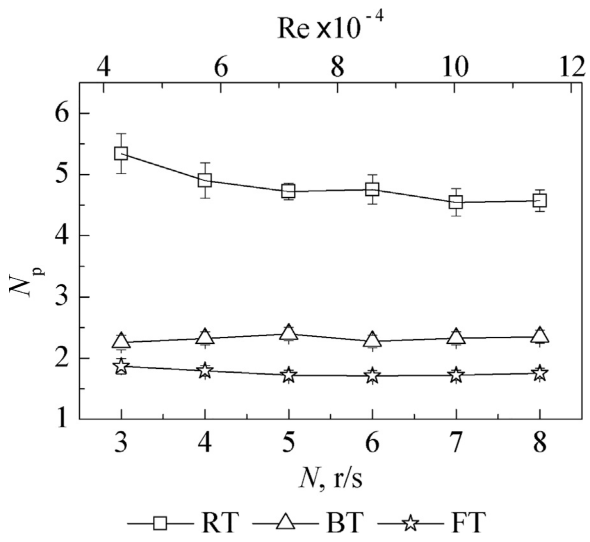

Fig. 4 – Power number (N_P) at various impeller speeds (N).

Fig. 4 shows the power number of the three impellers at various speeds and their corresponding Reynolds numbers. The power numbers of the BT and FT impellers were relatively stable (approximately 2.3 and 1.7 respectively) under the fully turbulent state and ungassed conditions, whereas that of the RT impeller was in the range of 4.5–5.3. The power number of the FT impeller was 26% lower than that of the BT impeller and 64% lower than that of the RT impeller. Reduction in power number is assumed to be mainly due to the increased vertex curvature of the FT blades. Myers et al. (1999) obtained a power number of approximately 5.5 for RT-6 impeller and a power number of 2.3 for BT-6 impeller. Other researchers have reported that the power number of RT impeller ranges from 4.2 to 6.0 (Pinelli et al., 2003). This disparity in power number is largely due to the fact that the impellers used by different research groups varied in terms of structure, size ratio, and dimensions.

3.2. *Relative power demand*

When air was sucked into the impeller, air accumulates in the low-pressure zone behind the blade and forms “gas cavities”. The power number of the impeller is significantly reduced under aeration conditions. Power reduction in the impeller under aeration condition reduces the radial pumping capacity, thereby reducing gas dispersion performance. On the one hand relative power demand (RPD) reflects the influence of low-pressure cavities on gas dispersion performance, on the

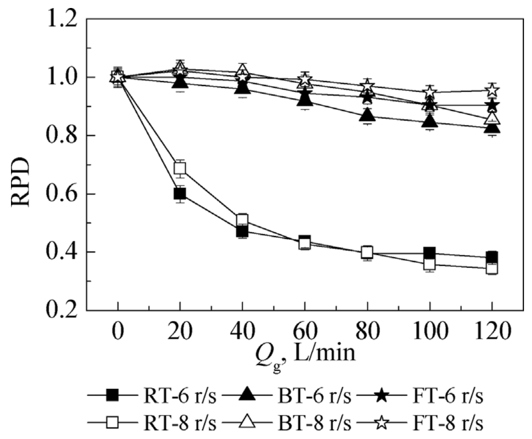

Fig. 5 – Relative power demand (RPD) at various gas flow rates (Q_g).

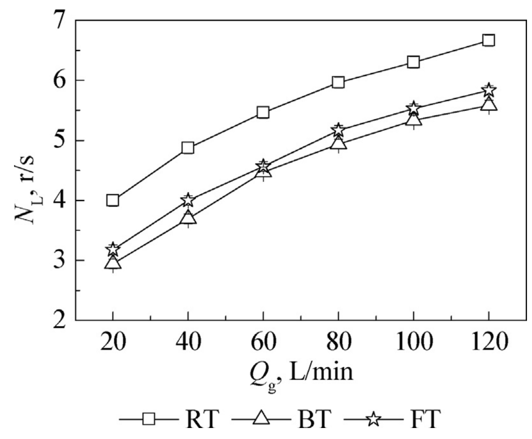

Fig. 6 – Critical dispersion speed (N_L) at various gas flow rates (Q_g).

other hand it is one of the characteristic parameters of radial flow impeller. The design for gas–liquid mass transfer must provide the calculated gassed power of the impeller, and this parameter is related to the power number and RPD (Bakker et al., 1994).

RPD is the ratio of gassed power to the ungassed power and was measured by increasing the gas flow rate at two fixed speeds (Fig. 5). RPD of the RT impeller decreased significantly with increased gas flow rate. When the gas flow rate was greater than 80 L/min, the RPD of the RT impeller was as low as 0.36, whereas that of the BT impeller was approximately 0.85. The RPD of the FT impeller was higher than that of BT impeller. The RPD of the FT impeller reached 0.90 at 6 r/s and 0.95 at 8 r/s. In summary, the RPD characteristic of the FT impeller was slightly better than that of the BT impeller, and both RPD values were significantly higher than the RPD of the RT impeller. The RPD of the FT impeller was close to the ideal value of 1.0 and thus bring great convenience to designers, as well as results in strong robustness under gassed and agitated operations.

Evaluating the performance of an impeller by power number and RPD only is insufficient. It is also necessary to consider the robustness (such as gas flooding occurs at the regular ranges of the superficial gas velocity), stability (such as the shaft axial runout during the gassed operation) and gas handling capacity of the impeller during operation. The power number of axial flow impellers is generally smaller than that of radial flow impellers. For example, the power number and RPD of a pitch blade turbine are 1.3 and 0.3, respectively, whereas those of Lightnin A315 are 0.75–0.8 and 0.7, respectively (Middleton and Smith, 2004). It can be concluded that in a single-phase system, the axial flow impellers could pump an increased flow rate under the same power input. Does this mean that axial flow impellers can handle a gas–liquid fluid more efficiently? It should be noted that axial flow impellers cannot be used as a bottom impeller in a multi-impeller agitation system. Downward axial flow impellers, such as pitch blade turbines and narrow-blade impellers, demonstrate a seriously unstable operation in gas–liquid systems. The RPD of the impeller would suffer a sharp drop in the transition state between indirect and direct loading as gas flow increases (Smith and Gao, 2001). The detrimental consequences of this phenomenon include fluctuation of process performance, rapid wear of seals and bearings, and high risk of shaft failure. Although axial flow wide-blade impellers (such as Lightnin A315 and Lightnin A320) are highly efficient in gas–liquid mass transfer, they are mostly used as upper impellers in multi-impeller systems.

3.3. *Critical dispersion speed*

Gas flow pattern depends on the regime of gas–impeller interaction. Three flow regimes exist in the vessel: flooding, loading, and complete dispersion (Lu and Chen, 1986). (1) In flooding, wherein the impeller is overwhelmed by gas and gas–liquid contact, mixing are very poor. (2) In loading, the impeller disperses the gas in the upper part of the vessel. (3) In complete dispersion, gas bubbles are distributed throughout the vessel, and a considerable amount of gas is recirculated back into the impeller. Flooding is detrimental to gas–liquid mass transfer and operational stability. Its occurrence is closely related to the structure of the impeller, impeller speed, and gas flow rate.

Critical dispersion speed is the impeller speed at which the flow pattern is transmitted from flooding to loading. To evaluate the gas handling capacity, we obtained the critical dispersion speed of the impellers at various gas flow rates (Fig. 6). The critical dispersion speeds of the BT and FT impellers were evidently lower than that of the RT impeller, indicating that the former two impellers could handle a higher gas volume than the RT impeller at the same speed. Moreover, the BT and FT impellers demonstrate better robustness and wide operation range because they are less likely to operate under a flooding condition. The critical dispersion speed of the FT impeller was slightly higher than that of the BT impeller possibly due to the larger actual sweeping diameter of the latter (Fig. 1).

Impellers with larger diameter can handle high volumes of gases (Takahashi et al., 2014). Given the small power number of the FT impeller, a designer may select a large diameter to obtain a higher gas handling capacity under the same power input. If the impeller speed is lower than the critical dispersion speed, the oxygen transfer performance of the fermenter will be adversely affected, especially the performance of the region below the impeller. It would lead to a heterogeneous dissolved oxygen environment in the bioreactor, and the respiration of the microorganisms in the local area will not be met; thus, such phenomenon is detrimental to the efficiency of the entire bioprocess.

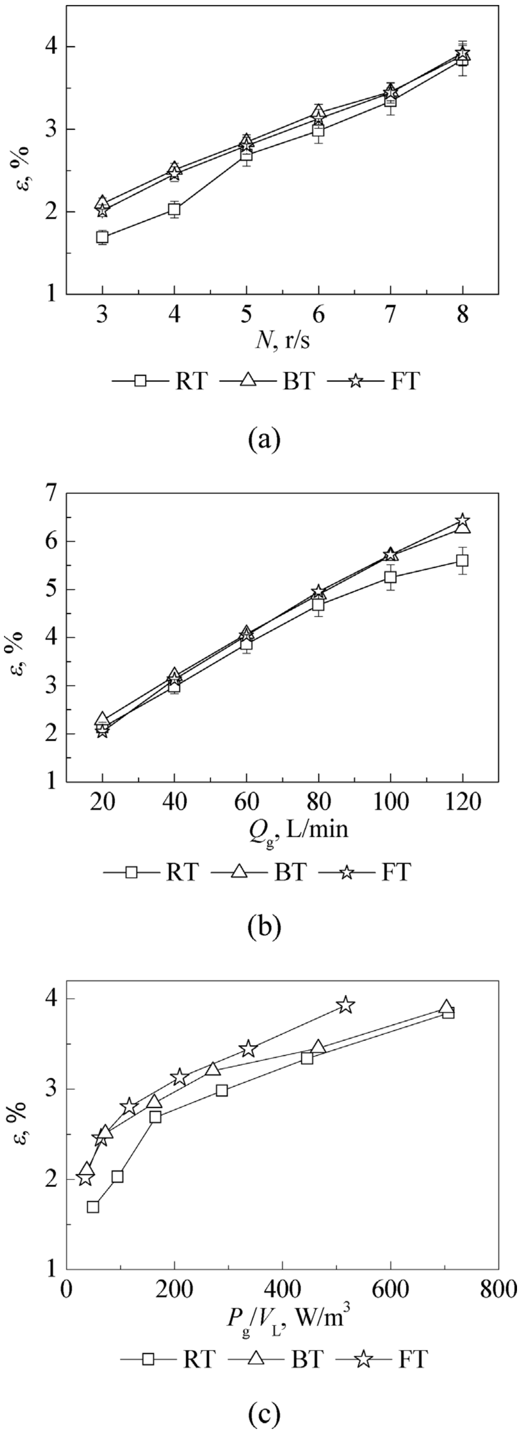

Fig. 7 – Gas holdup (ε) at (a) various impeller speeds (N) and Q_g = 40 L/min, (b) gas flow rates (Q_g) and N = 6 r/s, and (c) gassed power (P_g/V_L).

3.4. Gas holdup

Gas holdup is influenced by flow pattern and bubble distribution state. This parameter was measured at various speeds (Fig. 7a) and at various gas flow rates (Fig. 7b). Among the three impellers, the RT impeller showed the lowest gas holdup at a low speed or at a high gas flow rate because flooding occurred under these conditions. By contrast, flooding under these test conditions did not occur in the BT and FT impellers. The BT and FT impellers captured a greater amount of upward gas flow, and they pumped the gas out from their deep concaved blades. The gas holdup performance of the BT and FT impellers was very similar. As shown in Fig. 7c, FT impeller had a better gas holdup than the other two impellers at the same gassed power input.

The overall gas hold-up as a function of the impeller power and superficial gas velocity was expressed by the following relationship:

$$\varepsilon = k_1 \left(\frac{P_g}{V_L}\right)^{k_2} (v_s)^{k_3} \quad (7)$$

where k_1, k_2, and k_3 are constants which are specific for each impeller. The constants and the exponents in the equation also affect by various geometrical parameters of the impeller, such as the surface of the blade, D/T ratio, installation position, etc. Correlations obtained by regression of the experimental data for the each impeller are shown in Table 3. The exponents in Eq. (7) on (P_g/V_L) and (v_s) for the impellers were very similar to those previously published by Xie et al. (2014). Considering of the impeller configuration effect we add the power number and relative power demand in the gas hold-up data correlation. Using the experimental data of all the three impellers, the resulting correlation was given as follows:

$$\varepsilon = 0.225 \left(\frac{P_g}{V_L}\right)^{0.231} (v_s)^{0.602} (N_P \cdot RPD)^{-0.28} \quad (8)$$

with standard deviation of 5.51% and correlation coefficient of 0.976. The values of the $N_P \cdot RPD$ for the RT, BT and FT impeller were 2.24 ± 0.55, 1.96 ± 0.15 and 1.62 ± 0.07, respectively. It was indicated that the combined parameter $N_P \cdot RPD$ could well reflect the configuration difference and performance characteristics of the three impellers.

3.5. Volumetric oxygen transfer coefficient

Volumetric oxygen transfer coefficient (k_La) is a key parameter used to measure gas–liquid mass transfer performance. This parameter is related to factors such as impeller type, agitation power, gas flow rate, and physical and chemical properties of a liquid. The volumetric oxygen transfer coefficient was measured under various impeller speeds (Fig. 8a) and under various gas flow rates (Fig. 8b). The volumetric oxygen transfer coefficient obviously increased with increasing impeller speed and gas flow rate. As shown in Fig. 8c, the volumetric mass transfer coefficients of the RT, BT and FT impellers showed an increasing trend at the same gassed power input.

Fig. 8a shows that the volumetric oxygen transfer coefficients of the BT and FT impellers were slightly higher than that of the RT impeller under the same gas flow rate. Similar results were observed under various gas flow rates at the same speed (Fig. 8b). The FT impeller displayed a similar k_La to that of the BT impeller at the same speed and aeration conditions, but the power input of the FT impeller was lower than that of the BT impeller. Researchers have associated k_La with power per unit volume and gas flow rate in the absence of gas flooding (Linek et al., 2012; Labík et al., 2014). A higher power results in increased oxygen transfer coefficient in liquid phase, and the gas flow rate mainly influences the gas holdup, further affecting the total interface area of the bubbles in the flow field.

Table 3 – Constants k_1–k_6 defined by Eqs. (7) and (9) for correlation of gas holdup (ε) and volumetric oxygen transfer coefficient (k_La).

Impeller type	ε				k_La			
	k_1	k_2	k_3	R^2	k_4	k_5	k_6	R^2
Rushton turbine	0.147	0.298	0.648	0.993	0.0136	0.381	0.458	0.982
Bakker turbine	0.265	0.199	0.637	0.996	0.0113	0.388	0.410	0.994
Fan-shaped turbine	0.270	0.232	0.670	0.999	0.0174	0.361	0.451	0.992

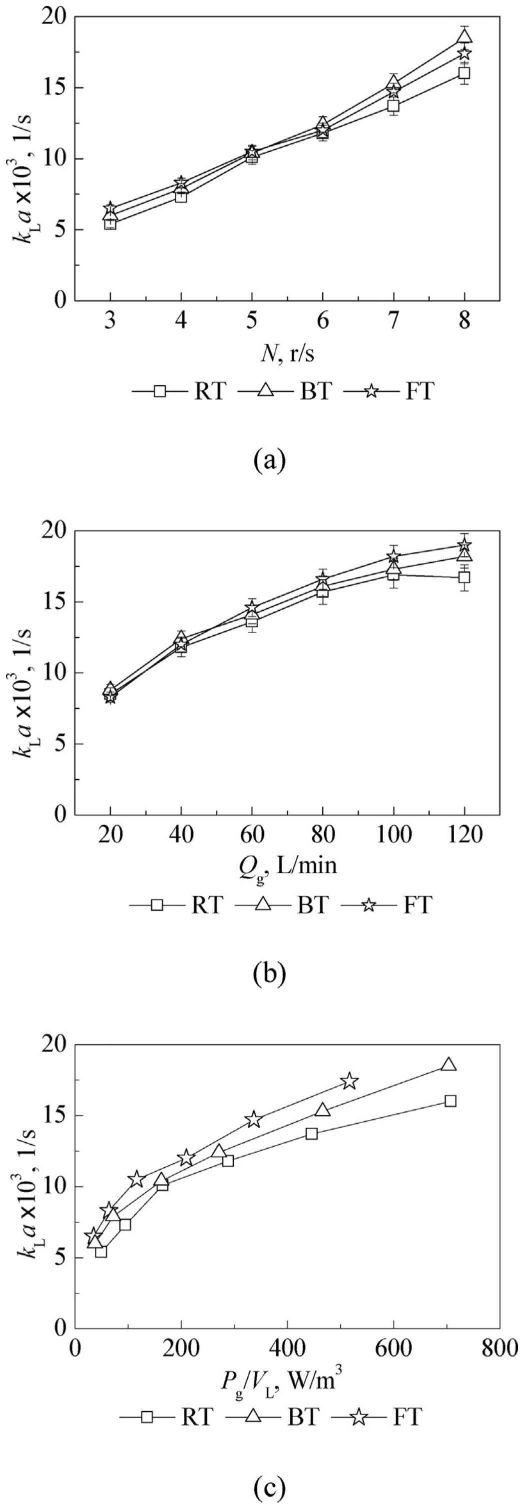

Fig. 8 – Volumetric oxygen transfer coefficient (k_La) at (a) various impeller speeds (N) and Q_g = 40 L/min, (b) gas flow rates (Q_g) and N = 6 r/s, and (c) gassed power (P_g/V_L).

The experimental volumetric oxygen transfer coefficient data was correlated as a function of the power input and gas superficial velocity by using the model as below,

$$k_La = k_4\left(\frac{P_g}{V_L}\right)^{k_5}(v_s)^{k_6} \tag{9}$$

Model parameters for different impellers are shown in Table 3. The power number and relative power demand were also added to correlate volumetric oxygen transfer coefficient data for the three impellers as follows:

$$k_La = 0.0137\left(\frac{P_g}{V_L}\right)^{0.372}(v_s)^{0.372}(N_P \cdot RPD)^{-0.4} \tag{10}$$

with standard deviation of 5.53% and correlation coefficient of 0.963.

The k_La was measured by the classical dynamic method in this work. Comparing with the dynamic pressure method, the resulting experimental data might be underestimated (Linek et al., 2012). Since the agitation experiments were carried out under the same reactor and operating conditions, the measurement error was systematic and would not apparently affect the performance comparison of the three impellers. According to the evaluation method by Moucha et al. (2012), we evaluated the effect of gas residence time in the gas holdup on k_La. At the gas superficial velocity of 3.2–19.0 mm/s and gas holdup of 1.7–6.4%, which were used in this work, the gas residence time in the gas holdup was 1.1–2.9 s. For the range of k_La (0.005–0.019 s^{-1}) measured by classic dynamic method, we obtain the weighting (w = 1.006–1.049) for the mass transfer effect and $(1 - w)$ = −0.006 to −0.049 for the gas holdup washout effect. It indicated that the k_La value really determines the liquid concentration profile shape under the mixing intensity of the experimental condition, while the effect of gas hold-up washout was negligible.

3.6. *Oxygen transfer efficiency*

The oxygen transfer efficiency of an impeller could be evaluated by determining the volumetric oxygen transfer coefficient under a certain power input. This evaluation is industrially significant as energy costs may be reduced when required operational objectives are met. Oxygen transfer efficiency (E) refers to the volume of fluid in which per unit energy could be dispersed by the impeller under aeration conditions. Oxygen transfer efficiency can be used to measure the ability and efficiency of an impeller to dissipate energy and disperse gas in a liquid. Oxygen transfer efficiency was evaluated at various speeds (Fig. 9a) and under various gas flow rates (Fig. 9b). The oxygen transfer efficiency of the three impellers significantly varied under different speeds and aeration conditions. The oxygen transfer efficiency decreased with increased impeller speed, whereas it increased under increasing gas flow rate. If bioreaction process requires a high oxygen uptake rate,

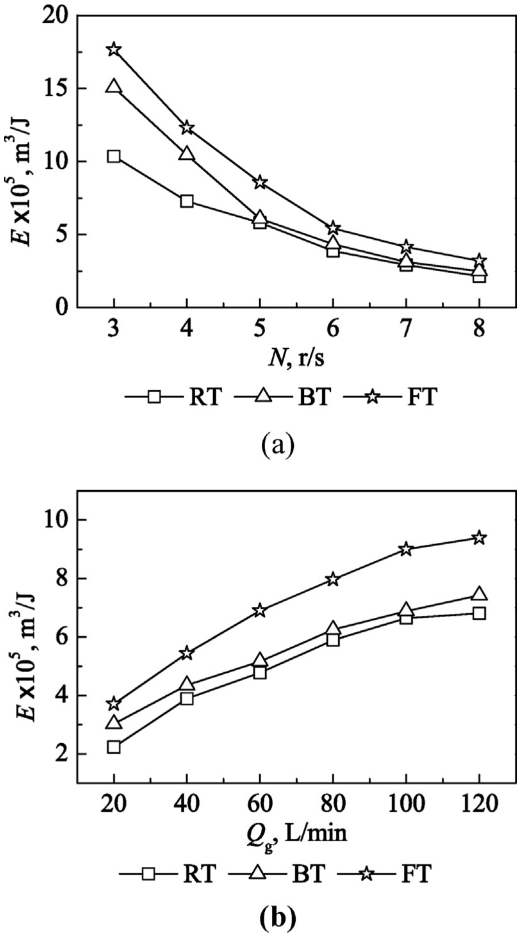

Fig. 9 – Oxygen transfer efficiency (E) at (a) various impeller speeds (N) and Q_g = 40 L/min, and (b) gas flow rates (Q_g) and N = 6 r/s.

then a high agitation power could satisfy such a requirement, resulting in reduced oxygen transfer efficiency. An increased gas flow rate is beneficial for an agitation system to achieve a more efficient gas dispersion performance. Given that an increased gas flow rate increases the power consumption of an air supply system, optimization of agitation and aeration conditions for optimum performance of the entire reaction system is therefore necessary. The correlation equations of the power of aeration (P_A) and agitation power under gassed condition (P_g) are as follows,

$$P_A = v_s \rho g V_L \tag{11}$$

$$P_g = RPD \cdot N_P \cdot \rho N^3 D^5 \tag{12}$$

where ρ is liquid density. Combine the above two equations into Eq. (9), we get

$$k_L a = k_4 \cdot \left(\frac{RPD \cdot N_P \cdot \rho N^3 D^5}{V_L}\right)^{k_5} \left(\frac{4Q_g}{\pi T^2}\right)^{k_6} \tag{13}$$

Increasing agitation speed or aeration rate can make $k_L a$ satisfy the requirement of biological reactions. As shown in the Eqs. (11)–(13), we can optimize and search an appropriate operational combination of agitation speed (N) and gas flow rate (Q_g), so that $k_L a$ achieve the target value while making $P_A + P_g$ minimum.

As shown in Fig. 9a, the oxygen transfer efficiency of the RT impeller was significantly lower than that of the two other impellers due to the occurrence of gas flooding at a low speed. As the speed was increased, the difference in oxygen transfer efficiency between the RT impeller and the two other impellers decreased with the disappearance of gas flooding. The oxygen transfer efficiency of the FT impeller was significantly higher than that of the BT and RT impellers under all the investigated speeds. This phenomenon was observed because the $k_L a$ of the FT impeller was close to that of the BT impeller under the same operating conditions, but the power of the FT impeller was considerably lower than that of the BT impeller. The oxygen transfer efficiency of the FT impeller was significantly higher by 35%–66% and 23%–34% than that of RT and BT impellers, respectively, with the various gas flow rates (Fig. 9b). Power consumption of a local area in the blade of the BT impeller and its contribution to gas mass transfer were deduced. The following conclusions were drawn: (1) the sweeping diameter of the BT impeller was larger than the diameter of the blade vertex line (Fig. 1). Moreover, the torque and power consumption in the outer edge of the blade were relatively high. The energy efficiency ratio is possibly lower in this area than in other areas. (2) The spatial surface of the FT blade may be better than that of the BT blade and could further promote gas dispersion efficiency.

4. Conclusions

A novel FT impeller assembly comprising parabolic annular sector concave blades was designed, and a new surface equation describing the concave blade was established. The power number of the FT impeller was approximately 1.7, which was lower by 26% and 64% than the power numbers of the BT and RT impellers, respectively. The RPD of the FT impeller reached 0.95, whereas that of BT impeller was close to 0.85. Although the power consumption of the FT impeller was relatively low at the same operation condition, the gas holdup and volumetric oxygen transfer coefficients were close to the BT and RT impellers. In summary, FT impeller has a convenient design, is an energy-saving assembly, demonstrates robustness during operation, and presents broad application prospects in gas dispersion. In order to deeply explain why FT impeller had better gas dispersion performance, further CFD simulation and explanation is currently underway and will be presented in next research paper.

Acknowledgements

Financial Support from Fundamental Research Funds for the Central Universities (JUSRP51632A, JUSRP51633B, 30915011101) and the Priority Academic Program Development of Jiangsu Higher Education Institutions, the 111 Project (No. 111-2-06) is gratefully acknowledged.

References

Bakker, A., 1998. Impeller assembly with asymmetric concave blades. US Patent, 5,791,780.
Bakker, A., Smith, J.M., Myers, K.J., 1994. How to disperse gases in liquids. Chem. Eng. 101, 98–102.
Devi, T.T., Kumar, B., 2013. Comparison of flow patterns of dual Rushton and CD-6 impellers. Theor. Found. Chem. Eng. 47, 344–355.
Fasano, J.B., Myers, K.J., Janz, E.E., 2011. Effect of geometric variations on the performance of gas dispersion impellers with semicircular blades. Can. J. Chem. Eng. 89, 961–968.

Galindo, E., Nienow, A.W., 1993. Performance of the scaba 6SRGT agitator in mixing of simulated xanthan gum broths. Chem. Eng. Technol. 16, 102–108.
Garcia-Ochoa, F., Gomez, E., 2009. Bioreactor scale-up and oxygen transfer rate in microbial processes: an overview. Biotechnol. Adv. 27, 153–176.
Gogate, P.R., Beenackers, A.A., Pandit, A.B., 2000. Multiple-impeller systems with a special emphasis on bioreactors: a critical review. Biochem. Eng. J. 6, 109–144.
Hjort, S., Skanberg, B., 1988. Impeller apparatus. US Patent, 4,779,990.
Labík, L., Vostal, R., Moucha, T., Rejl, F.J., Kordač, M., 2014. Volumetric mass transfer coefficient in multiple-impeller gas–liquid contactors. Scaling-up study for various impeller types. Chem. Eng. J. 240, 55–61.
Linek, V., Moucha, T., Rejl, F.J., Kordač, M., Hovorka, F., Opletal, M., Haidl, J., 2012. Power and mass transfer correlations for the design of multi-impeller gas–liquid contactors for non-coalescent electrolyte solutions. Chem. Eng. J. 209, 263–272.
Lu, W.M., Chen, H., 1986. Flooding and critical impeller speed for gas dispersion in aerated turbine-agitated vessels. Chem. Eng. J. 33, 57–62.
Middleton, J. C., Ramshaw, C., 1993. Agitators. US Patent, 5,198,156.
Middleton, J.C., Smith, J.M., 2004. Gas–liquid mixing in turbulent systems. In: Paul, E.L., Atienoobeng, V.A., Kresta, S.M. (Eds.), Handbook of Industrial Mixing: Science and Practice. John Wiley & Sons, Inc., New Jersey, pp. 585–638.
Moucha, T., Rejl, F.J., Kordač, M., Labík, L., 2012. Mass transfer characteristics of multiple-impeller fermenters for their design and scale-up. Biochem. Eng. J. 69, 17–27.
Myers, K.J., Thomas, A.J., Barker, A., Reeder, M.F., 1999. Performance of a gas dispersion impeller with vertically asymmetric blades. Chem. Eng. Res. Des. 77, 728–730.
Nienow, A.W., 1990. Agitators for mycelial fermentations. Trends Biotechnol. 8, 224–233.
Pinelli, D., Bakker, A., Myers, K.J., Reeder, M.F., Fasano, J., Magelli, F., 2003. Some features of a novel gas dispersion impeller in a dual-impeller configuration. Chem. Eng. Res. Des. 81, 448–454.
Rushton, J.H., Costich, E.W., Everett, H.J., 1950. Power characteristics of mixing impellers, part II. Chem. Eng. Prog. 46, 467–476.
Smith, J.M., Gao, Z., 2001. Power demand of gas dispersing impellers under high load conditions. Chem. Eng. Res. Des. 79, 575–580.
Takahashi, K., Tanimoto, I., Sekine, H., 2014. Gas dispersion in an agitated vessel equipped with large impeller. J. Chem. Eng. Jpn. 47, 717–721.
Tervasmäki, P., Latva, M.K., Taskila, S., Tanskanen, J., 2016. Mass transfer, gas hold-up and cell cultivation studies in a bottom agitated draft tube reactor and multiple impeller Rushton turbine configuration. Chem. Eng. Sci. 155, 83–98.
Van't Riet, K., Boom, J.M., Smith, J.M., 1976. Power consumption, impeller coalescence and recirculation in aerated vessels. Trans. Inst. Chem. Eng. 54, 124–131.
Van't Riet, K., Smith, J.M., 1975. The trailing vortex system produced by Rushton turbine agitators. Chem. Eng. Sci. 30, 1093–1105.
Xie, M., Xia, J., Zhou, Z., Chu, J., Zhuang, Y., Zhang, S., 2014. Flow pattern, mixing, gas hold-up and mass transfer coefficient of triple-impeller configurations in stirred tank bioreactors. Ind. Eng. Chem. Res. 53, 5941–5953.
Zheng, Z., Sun, D., Zhan, X., Gao, M., 2017. Gas–liquid dispersion impeller assembly with annular-sector-shaped concave blades. US Patent Application no. 15, 548, 080.